Available online at www.sciencedirect.com
SCIENCE DIRECT®
International Journal of Heat and Fluid Flow 26 (2005) 80–91
International Journal of HEAT AND FLUID FLOW
www.elsevier.com/locate/ijhff

Numerical study of convective heat transfer from an array of parallel bluff plates

E. Velayati, M. Yaghoubi *

Mechanical Engineering Department, School of Engineering Shiraz University, Shiraz, Iran

Received 24 March 2004; accepted 7 May 2004
Available online 1 July 2004

Abstract

The turbulent fluid flow and heat transfer characteristics of heated rectangular plates such as fins mounted over a surface are investigated by numerical simulation using a finite-volume method. The investigation is performed taking into account effects of variation of the fin blockage ratio and flow Reynolds number. These parameters were changed to find their effects on reattachment position, velocity vector field, pressure distribution, friction coefficient and overall Nusselt number along the block surfaces. The governing equations are the continuity, momentum and energy equations with RNG based k–ε turbulence model. The temperature field in the block's mantle and on its outer surface was obtained solving the Fourier's conduction equation. Numerical validation is made by comparing the results with experimental measurements and good agreement was observed. Variation of average convection heat transfer coefficient over the block surfaces is identified and a correlation of the form $\overline{Nu} = 0.126Re^{0.68}(1 + 2.13\mathrm{Br})$ for average overall heat transfer coefficient from the blocks is presented. Considering these blocks to act as fins, a correlation for overall fin efficiency as $\eta_f = 2.823Re^{-0.14}\mathrm{Br}^{-0.0526}$ is also developed.
© 2004 Elsevier Inc. All rights reserved.

Keywords: Bluff plates; Turbulent flow; Conjugate heat transfer; Separation; Reattachment; Secondary flows; Fin efficiency

1. Introduction

Recirculating flows arising from the separation of a boundary layer and its subsequent reattachment occur in many situations of practical interest such as combustion chambers, gas turbine blades, heat exchangers, large ducts, electronic devices, vehicles motion and wind flow around parallel buildings. These systems either resemble parallel blocks or certain elements that are introduced to enhance heat transfer between incoming fluid and a corresponding base plate. For example, blocks or fins over heat generating elements, blocks over surfaces in heat exchangers, etc. with free stream conditions. The incoming fluid which is mostly air blows from a near by fan or air blows through a large chamber with rectangular blocks over its surfaces. For some applications, the plates are relatively thick and the flow is not of a boundary layer type, being accompanied by fluid separation and reattachment. In these cases, flow recirculation influences the rate of heat transfer from the body, and accurate knowledge of fluid flow and heat transfer between these prisms and ambient air improves design and construction, increases life-time, optimizes material consumption, reduces the space required to install these elements, and eliminates hot spots to facilitate better ways of cooling heat generating components. The nature of flow around two-dimensional finite thick rectangular plates is sketched in Fig. 1. As the flow moves from left to right, the decreases in its velocity cause a positive pressure gradient on the front surface. The addition of pressure in the stream-wise direction and adverse pressure on the side surfaces causes the flow to separate from the leading edge, and after a distance, to reattach to the plate, forming a recirculation bubble within which there is a reverse pressure distribution. Subsequently, boundary layer growth begins and approaches to the end of the plate surface and leaves the plate forming a wake behind the block. The mixing region between the separation point and the reattachment

* Corresponding author. Tel.: +98-711-2303051; fax: +98-711-2301672.
E-mail address: yaghoub@shirazu.ac.ir (M. Yaghoubi).

0142-727X/$ - see front matter © 2004 Elsevier Inc. All rights reserved.
doi:10.1016/j.ijheatfluidflow.2004.05.001

Nomenclature

A_c	fin cross-section area
Ar	aspect ratio (L/D)
Br	blockage ratio (D/W)
c_μ, c_1, c_2	coefficients in turbulence model, 0.085, 1.42, 1.68
C_f	friction factor coefficient
C_p	specific heat
D, H, L, W	plate thickness, height, length and spacing
G	shear generation, $\mu_t(u_{i,j}+u_{j,i})u_{ij}$
h	convection heat transfer coefficient
Hr	height ratio, (H/D)
K	thermal conductivity of solid
k	turbulent kinetic energy, $\overline{u_i'u_i'}/2$
Nu, Nu_L	Nusselt number, $(hD)/\lambda, (hL)/\lambda$
p	pressure
P	fin perimeter
Pr	Prandtl number
Re, Re_L	Reynolds number, $(U_\infty D)/v, (U_\infty L)/v$
S_{ij}	mean strain rate tensor, $(\mu_{i,j}+\mu_{j,i})/2$
S	$\sqrt{2S_{ij}S_{ij}} = \sqrt{G/u}$,
T	temperature
T_s	fin surface temperature
u_i	index notation of velocity components
$\overline{u_i'u_j'}, \overline{u_i'T'}$	turbulent Reynolds stress tensor and heat flux
x, y, z	directions of rectangular coordinate
Xr, Yr	length and altitude of center of the reattachment region

Greeks

α	fluid thermal diffusivity, angle of attack
β	parameter in RNG k–ε mode, 0.012
δ_{ij}	Kronecker delta function
ε	turbulent dissipation rate, $\mu(\overline{u_{i,j}'u_{i,j}'})/\rho$
η, η_0	parameters in RNG k–ε mode, Sk/ε, 4.38
λ, λ_t	total and turbulent thermal conductivity of fluid, $(\lambda_0+\lambda_t), (C_p\mu_t/\sigma_t)$
λ_0	laminar thermal conductivity of fluid
μ, μ_t	total and eddy viscosity, $(\mu_0+\mu_t), (c_\mu\rho k^2/\varepsilon)$
μ_0	laminar viscosity
v	fluid kinematic viscosity
ρ	fluid density
σ_t	turbulent Prandtl number
$\sigma_k, \sigma_\varepsilon$	turbulent Prandtl numbers for diffusion of k and ε
τ_w	wall shear stress

Subscripts

∞	uniform free-stream condition
i	$i = 1, 2, 3$ Cartesian coordinate
i, j, k	tensor notation
$()_{,j}$	derivative respect to j direction

Superscripts

$(\bar{})$	time average component of turbulent parameter
$()'$	fluctuating component of turbulent parameter

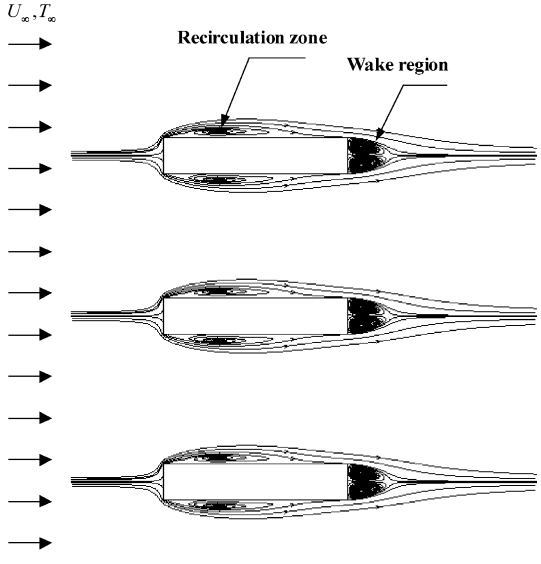

Fig. 1. Fluid flow around an array of 2D bluff plates, Ar = 5.

point plays an important role in heat and mass transfer processes.

Theoretical and experimental analyses of fluid flow and heat transfer from horizontal parallel plates and in rectangular thin ducts have been reported in detail. These studies are either for two-dimensional semi-infinite plates or from two-dimensional thick finite plates. Experimental studies of McCormick et al. (1984) revealed that, in general, details of heat transfer and pressure variations in separated flows depend upon the prior history of the upstream flow. For two-dimensional cases, potential flow influences are much more important and boundary layer effects are typically negligible. That is, separation occurs at a corner (because of leading-edge bluntness) rather than because a boundary layer lacking in momentum encounters a sufficiently large adverse pressure gradient. The pressure field inside the separated flow region is then determined largely by the outer stream flow passing around the body.

For a single thick plate with semi-infinite length, analysis is also extensive. Experimental studies of Ota

and Kato (1991) and the measurements of Ota and Ohi (1995) of turbulent heat transfer over a two-dimensional blunt plate for $Re = 5800$ show that the Nusselt number reaches a maximum at about 4.3 plate thickness while the attachment point was located at 4.1 plate thickness. Djilali and his co-workers performed a series of both numerical and experimental studies of turbulent flow over a bluff rectangular plate. In the experimental part, Djilali and Gartshore (1991a) showed that the reattachment length and pressure distribution remained unchanged over the Reynolds number range 2.5×10^4 to 9×10^4. In the numerical computations, Djilali et al. (1991b) used a modified standard k–ε turbulence model and a variant that incorporates the curvature correction. Their results show that the prediction of reattachment is very sensitive to the numerical scheme and to turbulence modeling. They used two different discretization methods: hybrid differencing (HD) and bounded skew hybrid differencing (BSHD) schemes. It was found that BSHD, which has a higher differencing order, had better agreement for a reattachment length of 4.3 plate thickness with an experimental measurement of 4.7D.

Recent experimental studies for two-dimensional flow have been presented by Igarashi and Mayumi (2001) and Hwang et al. (2001). Experimental studies of Igarashi and Mayumi (2001) on fluid flow and heat transfer phenomena around a rectangular block with an aspect ratio of 5 were carried out for Reynolds numbers in the range of $2.6\times10^3 < Re < 1.28\times10^4$. The angle of attack a was varied from 0° to 20°. They proposed an empirical formula for the Nusselt number as $\overline{Nu} = 0.085Re^{2/3}$ (for $\alpha = 0$–10° and $Re > 4\times10^3$).

For blocks attached onto a base surface, such as a ribbed surface, finite fins mounted over an engine, parallel boards attached to a plate, etc., the flow over each block is no longer two-dimensional, and reattachment strongly depends on the geometry and flow condition. For such geometries, for a row-dependent case, Sparrow et al. (1982) reported experimental results for turbulent flow for arrays of heat generating rectangular modules deployed along one wall of a flat rectangular duct. Experiments were performed with fully populated arrays, arrays in which there were missing modules, arrays where barriers were implanted to obtain heat transfer enhancement, and arrays in which there was both a missing module and a barrier. Row independent results were obtained for the 5th and all subsequent rows. Missing modules result in enhancement of heat transfer. For fully populated array without barriers, a row-independent (fully developed) heat transfer coefficient was obtained. The fully developed Nusselt number for heat transfer (to air) was correlated as $\overline{Nu} = 0.0935Re_H^{0.72}$, where the Reynolds number is based on the vertical space above the blocks. Meinders and Hanjalic (1999) reported the local heat transfer for a matrix of equidistant cubes mounted on the floor of a parallel plate channel. In this study, the surface temperature of an internally heated cubical element was measured with infrared thermography. Most of the previous studies belong to ribs in pipes or ducts, which have been reviewed by Kim and Kim (2002).

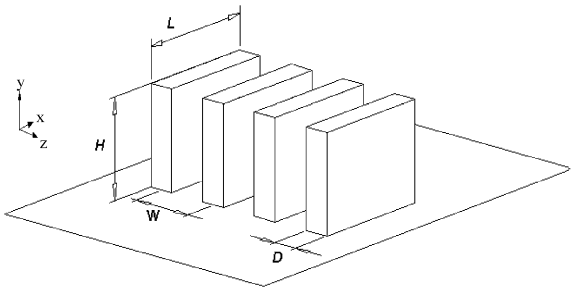

Fig. 2. Parallel 3D finite bluff plates.

Understanding the details of flow and heat transfer over blunt flat plates is very important. Furthermore, three-dimensional measurements of such a complicated flow are not easy to conduct, but numerical analysis may be appropriate for understanding details of heat transfer mechanisms when the fins are parallel to the free-stream flow. For such cases, upstream flow, geometric details and conduction within the fins will have a strong effect on the rate of heat transfer and pressure drop through the blocks. For a single array of blocks the flow boundary conditions are no longer periodic with developed conditions as described by Sparrow et al. (1982). Turbulent flow with combined conduction in parallel blocks and convection heat transfer within the fluid such as shown in Fig. 2 has not yet been reported. In this geometry, the parameters which play important roles are known to be block or fin thickness (D), fin length (L), fin spacing (W), fin height (H). For such geometries the flow structure is complex due to the interaction of viscous layers over the base with the recirculation bubble over the leading edge as well as the effects of the flow over the top surface and free-stream interaction with flow between the plates. The part of the flow attached to the fin base damps the circulation and produces swirl flow through the duct. In this study, air with constant temperature and uniform velocity approaches the blocks and flow will be assumed turbulent with constant physical properties.

2. Governing equations

The governing equations for the three-dimensional steady state incompressible fluid flow are as follows:

2.1. Time-averaged equations

By applying time-averaging procedures to conservation equations, the equations that govern the mean-flow quantities, u_i, p and T, for turbulent flow are:

$$u_{i,j} = 0 \tag{1a}$$

$$\rho(u_j u_{i,j}) = -p_{,i} + |\mu(u_{i,j} + u_{j,i}) - \rho\overline{u_i' u_j'}|_j \tag{1b}$$

$$\rho C_p(u_j T_{,j}) = (\lambda T_{,j} - \rho C_p \overline{u_j' T'})_{,j} \tag{1c}$$

Applying the Boussinesq approximation, the Reynolds stress tensor and turbulent heat fluxes are:

$$-\rho\overline{u_i' u_j'} = 2\mu_t S_{ij} - \frac{2}{3}\rho k \delta_{ij} \tag{2a}$$

$$-\rho C_p \overline{u_i' T'} = \lambda_t T_{,j} \tag{2b}$$

2.2. RNG based k–ε turbulent model

In k–ε models, the turbulence field is characterized in terms of turbulent kinetic energy (k) and viscous dissipation rate of turbulent kinetic energy (ε). Yakhot and Orszag (1986) proposed a variant of the k–ε model such that its performance characteristics were improved relative to the standard model. The RNG turbulence model is more responsive to the effects of rapid strain and streamline curvature, flow separation, reattachment and recirculation than the standard k–ε model. The forms of the k and ε equations of the RNG model without buoyancy effects are as follows:

$$\rho u_j k_{,j} = \left(\left(\mu + \frac{\mu_t}{\sigma_k}\right)k_{,j}\right)_{,j} + G - \rho\varepsilon \tag{3a}$$

$$\rho u_j \varepsilon_{,j} = \left(\left(\mu + \frac{\mu_t}{\sigma_\varepsilon}\right)\varepsilon_{,j}\right)_{,j} + c_1 \frac{\varepsilon}{k} G - \frac{c_\mu \eta^3 (1 - \eta/\eta_0)}{1 + \beta\eta^3} \frac{\varepsilon^2}{k} - c_2 \rho \frac{\varepsilon^2}{k} \tag{3b}$$

The primary coefficients of the RNG model are provided by Yakhot et al. (1992). The terms $c_1 G(\varepsilon/k)$ and $c_2\rho(\varepsilon^2/k)$ in (3b) represent, respectively, the shear generation and viscous dissipation of ε. The extra term in (3b) employs the parameter η, which represents the ratio of characteristic time scales of turbulence and the mean flow fields, defined by $\eta = Sk/\varepsilon$. It can be shown that η is a function of the ratio of generation to dissipation of k and can be written as:

$$\eta = \sqrt{c_\mu^{-1}(G/\rho\varepsilon)} \tag{3c}$$

The temperature field in the block's mantle and on its outer surface (providing the boundary condition for the convection) was obtained by solving the Fourier's heat conduction equation simultaneously with heat convection in the fluid. This coupling of the temperature field and computation of the instantaneous block surface temperature is assumed by including conduction heat flux from the solid to the interface of the nearby control volume of the fluid cell. For heat conduction in the blocks, Fourier's equation was employed as:

$$T_{,jj} = 0 \tag{4}$$

3. Boundary conditions

To carry out numerical computations, several attempts were made to identify the appropriate domain around the blocks. First, a complete block was considered and computations performed for the full domain grids. For the considered conditions (Reynolds numbers and blockage ratios) completely symmetric results were obtained that shows a steady state regime. For low blockage ratios there was possibility of flow transition to unsteady conditions. In order to find any differences in the flow regime, the flow between two half section of blocks was simulated again. It was found that even for such condition, the flow is symmetric and any possibility to unsteadiness was not considerable. Based on this result, for the rest of computations, only a half section of a block was selected as illustrated in Fig. 3. For plane ABba, at the inlet boundary, uniform flow conditions are imposed for all variables using $u_{in} = U_\infty$, $v_{in} = 0$ and $w_{in} = 0$, $T_{in} = T_\infty$ and $k_{in} = 1.5 \times 10^{-6} U_\infty^2$. The inlet dissipation rate is estimated as $\varepsilon_{in} = k_{in}^{1.5}/(4.46 \times 10^{-1} D)$. Across the outlet, plane CDdc far from the plate, zero gradients of variables in the stream-wise direction, $\partial()/\partial x = 0$, are imposed.

Although this boundary condition is valid for fully developed flow, its use in other flow conditions is also permissible for computational convenient provided the outlet boundary is located in a region where the flow is in the downstream direction and sufficiently far from the

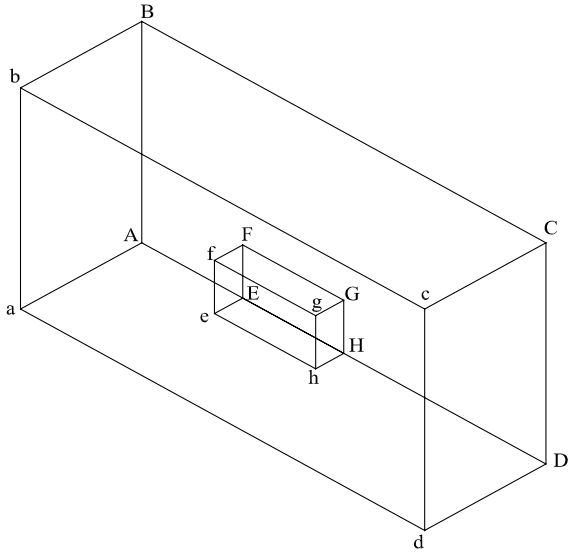

Fig. 3. Computational domain.

region of interest. For plane BCcb, a free-stream condition is assumed. The free-stream temperature is assumed to be 25 °C, the base surface of the blocks, plane HheE, is assumed to be at 75 °C and the base plate surface is assumed insulated.

For planes AEFGHDCB, FGHE and abcd, symmetry conditions are assumed so that on these planes zero cross-stream gradient condition, $\partial()/\partial z = 0$ is specified with $w = 0$. For solid surfaces, the base plate AEehHDda and the block surfaces fghe, FfeE, FfgG and GHhg, the near wall values for the parallel velocity components, temperature, the turbulent kinetic energy and its dissipation rate are determined from the standard log-law based wall function (Launder and Spalding (1974)) where in this model no-slip boundary condition will be imposed over the wall surfaces. The base plate, AEehHDda, will not have any contribution to heat transfer, because it will be assumed adiabatic.

4. Computational scheme

4.1. Domain geometry and grid size

The domain used in these calculations consist of an entrance region, an exit plane and the upper free-stream surface which should be selected sufficiently far from the block surfaces that the results become independent of the boundary positions. However for the upstream plane, the effect of the boundary layer development over the base plane may have a slight influence. But such distance is needed because the flow is actually not uniform over the front edge of the rectangles. In the present conditions, several tests were made and using the experience of previous studies (Yaghoubi et al. (2002)), the computational domain was chosen as illustrated in Fig. 3, where it extends $15D$ upstream, $40D$ downstream and the domain height is taken as $6H$. The blocks tested in this analogy are assumed to have an aspect ratio of 5, similar to the experimental studies carried out by Igarashi and Mayumi (2001).

The next step is selection of appropriate grid point numbers in the three-dimensional region such that the solution becomes independent of grid density. The grid is chosen to be dense near the plate and a typical grid is shown in Fig. 4. Grid independence was studied by changing the number of grids in all three dimensions and examining the corresponding predictions of flow field and pressure coefficient, friction factor and Nusselt number. Five different grids were tested and it was found that for each geometry and Reynolds number, special consideration should be made to study the independence of predicted flow on grid size and distribution. However, due to sharp corners and mixing of bubbles with boundary layers, several grid distributions were studied. For each grid the average friction coefficient, average Nusselt number and length (center position) of the reattachment region over the plane side surface is determined. Typical calculations are presented in Table 1. It was found that for $Re = 1 \times 10^4$ and $\mathrm{Br} = 20\%$, a grid of $165\times88\times32$ such as presented in Fig. 4, produced grid independent flow through the blocks, in terms of the mentioned flow parameters (see Table 2).

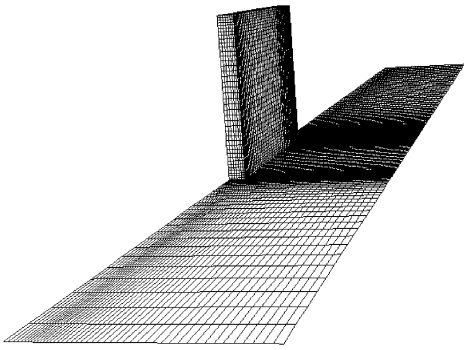

Fig. 4. Typical grid distribution.

Table 1
Grid independency of the results

Grids	$\overline{C_f}$	$\overline{Nu}$	Xr/D
$105\times60\times20$	0.00824	79.40	4.83
$125\times70\times24$	0.00767	84.42	4.595
$145\times80\times28$	0.00724	88.67	4.328
$165\times88\times32$	0.00688	93.19	4.136
$180\times95\times36$	0.00678	94.36	4.077

Table 2
Various cases simulated

Parameter	Values
$Re = U_\infty D/v$	5×10^3, 5×10^4, 2×10^4, 3×10^4
$\mathrm{Br} = D/W$	10%, 15%, 20%, 25%
$\mathrm{Hr} = H/D$	5
$\mathrm{Ar} = L/D$	5

4.2. Computational procedure

The governing equations for turbulent three-dimensional flow are solved using the *finite volume* discretization technique, in which the control volume cells for velocity components are staggered with respect to the main control volume cells using the *SIMPLEC* pressure–velocity coupling algorithm developed by Vandoormaal and Raithby (1984).

4.3. Validation

To assess the present computational method, two-dimensional experimental studies on fluid flow and heat transfer characteristics around a rectangular cylinder by

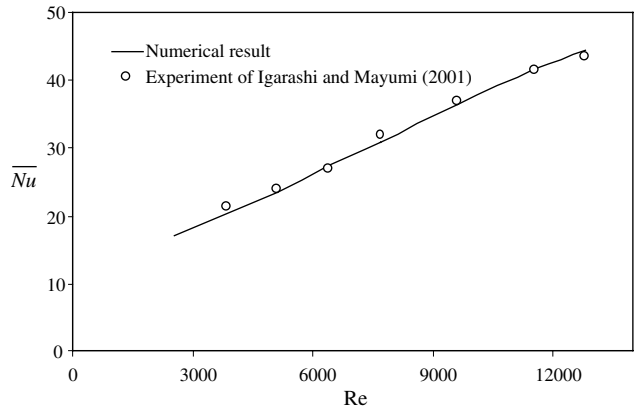

Fig. 5. Comparison of average Nusselt number over the plates with Br = 6.6%, Ar = 5.

Igarashi and Mayumi (2001) were used. In this respect, the block aspect ratio is 5 and its blockage ratio 6.6% . Free-stream velocity was varied from 4 to 20 (m/s), which corresponded to Reynolds number, Re in the range 2.56×10^3 to 1.28×10^4, and free-stream turbulence intensity was chosen to be 0.4%. Also the temperature of the free-stream is nearly 20 °C, similar to experiments of Igarashi and Mayumi (2001). For the test model, a constant heat flux condition was considered. Numerical values of the average Nusselt number over the block surfaces was determined by calculating the average convective coefficient of all surface grids over the rectangular plate for similar flow conditions and the results are compared with the experimental measurements of Igarashi and Mayumi (2001) in Fig. 5. Very good agreement is observed for the range of considered Reynolds numbers.

5. Results and discussions

For an array of parallel rectangles, several computations were carried out to determine fluid flow, pressure field through the blocks or fins, conjugate conduction heat transfer and temperature distribution in the fins, and fluid convective heat transfer from blocks to the ambient flow. Calculation was performed for the cases presented in Table 2 (for $Pr = 0.7$).

5.1. Fluid flow

The flow field for the configuration shown in Fig. 2 is three-dimensional and can be divided into three regions; first the upstream section where the flow approaches nearly uniformly the leading edges of the plates. In this zone the flow splits into two parts as it approaches the plates, with a stagnation point at the forward face of the plate. The second region is between the plates where the base plate contributes to boundary layer development and flow separation leads to recirculation and reattachment over the plates and their interaction generates swirling motion within each channel. The third region is the fluid flow downstream from the rectangles, where a recirculation bubble behind the plate interacts with boundary layer development over the base plate. On the sides of the plate surfaces and in the leeward position, the size of the bubble varies with height. Typical fluid particle paths around the plates at different elevations from $0.1H$ to $0.9H$ are shown in Fig. 6. For this case, the reattachment position changes with height over the block side surfaces, while no reattachment occurred near the base plate and upper surface. For this region the center of the reattachment is placed at about $0.41H$. Fluid flow is strongly affected by the presence of the base

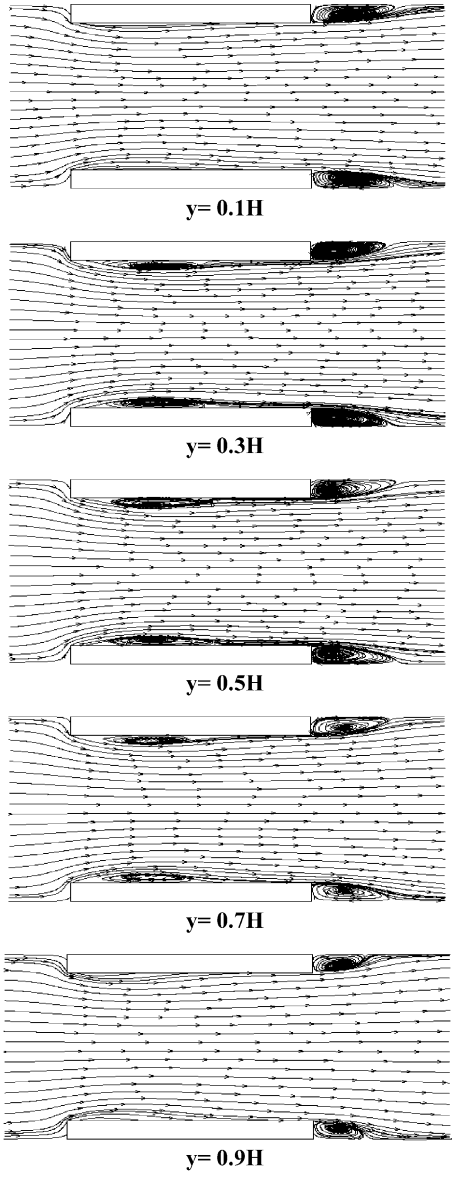

Fig. 6. Fluid particle paths around an array of plates at different heights, Hr = 5, Br = 20%, Ar = 5, $Re = 1 \times 10^4$.

plate and the free-stream above the fins and flow is strongly three-dimensional. Flow separation at the corners and recirculation over the fin surfaces, both at the top surface and the side surfaces has created a unique fluid flow, which is completely different from those in two-dimensional studies. Circulation behind the blocks is also visible, but far downstream, the effect of the blocks on the flow diminishes at such height ratio. Fig. 6 demonstrates that the flow changes at different height between blocks, with no recirculation near the base plate. For increasing heights, the flow over the top surface dominates, pushing down the bubble and mixing layer and preventing bubble formation near the block upper edge. A similar phenomenon is observed behind the plate.

In a turbulent flow in a straight duct of non-circular cross-section, a transverse mean flow exists when the flow is fully developed. This transverse flow, commonly known as the secondary flow, brings the fluids into complex lateral spiral motions as superimposed on the axial mean flow. Although the magnitude of the secondary flow scarcely amounts to a few percent of the bulk velocity, its presence displaces the lines of constant axial mean velocity considerably toward the corners, yielding a comprehensively high velocity field there. Flow through finite parallel blocks attached over a surface is also rotational and secondary flow by means of cross stream-wise velocity components, produced different flow patterns than those of parallel plates without attachment to a base plate. Secondary flow moves the fluid toward the corner along the plate side surface, over the base, and then outward in the mid-plane section due to symmetry with the opposite secondary flow. The direction of rotation in the mid-span section of the blocks is very similar to those reported by Shah and Bhatti (1987), which is presented for the mid-plane of close rectangular ducts in fully developed flow. The strength of the swirl reduces in the downstream direction, which corresponds to the weakness of distortion due to blocks in the flow fluid. A schematic of the secondary flow patterns between the plates for different Reynolds numbers is presented in Fig. 7. Swirling flows has a high gradient near the leading edge, the plate surface and the corner. Swirling motion mixes the boundary layer on the base with the bubble over the block side surfaces, resulting in a downward movement of the bubble and reattachment position. The boundary layer over the base plate opposes the recirculating bubbles that are formed over the plate side surfaces and eliminate flow reattachment over the block surfaces near the base plate as shown also in Fig. 6.

Typical 3D contours of the pressure field are illustrated in Fig. 8. The pattern of pressure distribution is not the same for different Reynolds number, however, the pressure field is high on the forward faces, and reduces behind the blocks as well as in the recirculation

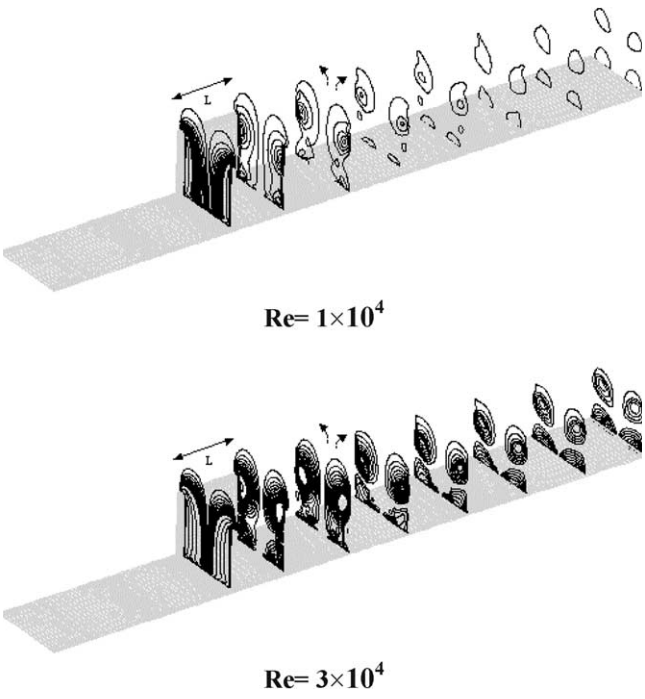

Fig. 7. Secondary flow distribution in various sections of stream-wise direction, Hr = 5, Br = 15%, Ar = 5.

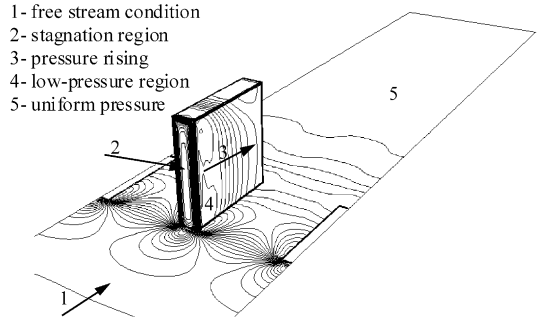

Fig. 8. Typical 3D contours of pressure over the plate, Hr = 5, Br = 20%, Ar = 5 and $Re = 1 \times 10^4$.

region. Pressure is uniform on upstream, downstream and far height above the blocks.

For parallel blocks, the position of reattachment over the side faces is important for studies of friction factor, pressure distribution and heat transfer, because the maximum value of heat transfer occurs around this region.

Consequently, accurate knowledge of this position is very important in heat transfer processes. Fig. 9 illustrates the center position of the reattachment region, where its length enlarges with increasing Reynolds number and reduces with increasing blockage ratio. Similar effects were observed for laminar flow by Yaghoubi et al. (2002). Also the height of the reattachment region decreases with increasing Reynolds

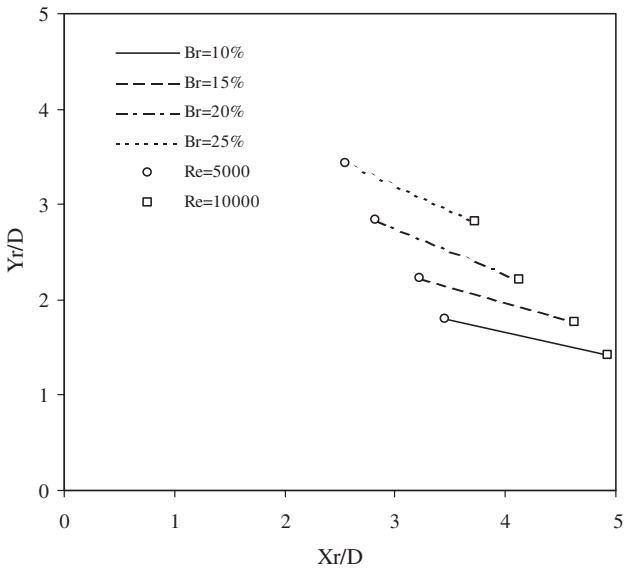

Fig. 9. Position of the reattachment region over the plate, Hr = 5, Ar = 5.

number and increases with an increase of the blockage ratio. This means that the bubble moves upward when the block separation is reduced and hence on increasing blockage ratio. It should also be noted that reattachment does not happen for high Reynolds number and also at low blockage ratios.

Variation of the flow field over the plate surface is accompanied by a shear stress distribution, which depends strongly on Reynolds number and plate blockage ratios. A typical surface shear stress field over the plate is illustrated in Fig. 10. The wall shear stress distribution is strongly three-dimensional. The shear layers get separated at the front edge, and then reattach over the plane surface and the separation bubbles are formed on the plate surface. The separation line appears in the location where separation bubbles are formed. This separation line is not a straight line. Fig. 10 shows the separation and reattachment regions over the side surface for Reynolds numbers 5×10^3 to 3×10^4. The region of flow reattachment area corresponds to zero wall shear stress an friction factor coefficient. These figures show that the flow reattachment region is moved to the end of the block with increasing Reynolds number as indicated in Fig. 9. These figures also show that reattachment will not occur for Reynolds number equal to and greater than 2×10^4.

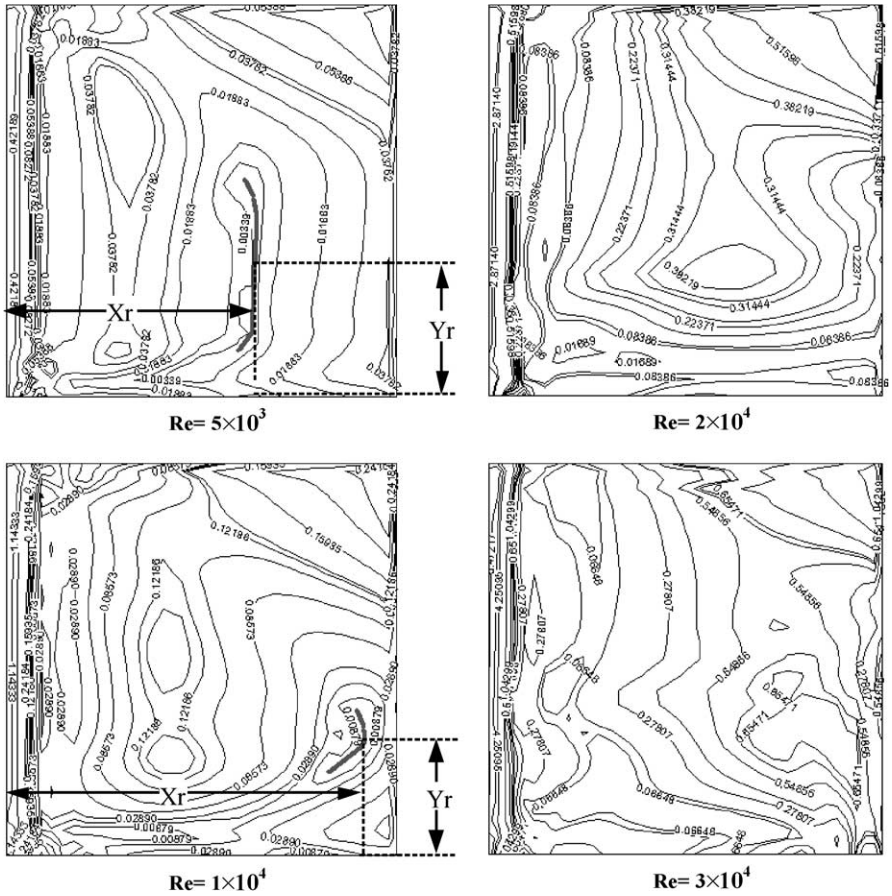

Fig. 10. Typical 2D contours ofwall shear stress over the plate, Hr = 5, Br = 15%, Ar = 5 ((●) reattachment region).

The average friction factor coefficient is calculated by:

$$\overline{C_f} = \frac{\bar{\tau}_w}{\frac{1}{2}\rho U_\infty^2} \quad (5)$$

where $\bar{\tau}_w$ the average wall shear stress over the block side surface. For the studies considered, wall shear stress is determined over the surface and its average value is calculated for each condition. Variation of average friction factor coefficient ($\overline{C_f}$) versus Reynolds number, in different blockage ratios over the side plate, is illustrated in Fig. 11. Comparison of the results with a standard correlation (Incropera and DeWitt, 1996) for thin plate shows good trends. Increasing blockage ratio enhances the friction coefficient. For all cases, the average friction factor coefficient decreases with increasing Reynolds number, which is similar to the flow over flat plates.

5.2. Heat transfer

The dynamics of flow and convection heat transfer are strongly three-dimensional and the average convection heat transfer coefficient is closely related to the fin spacing and Reynolds number. Heat transfer from the plate depends on the temperature field around the plate and variation of temperature over the plate surfaces. A typical three-dimensional temperature field for constant temperature of the plate's base surface is presented in Fig. 12. The area of dense temperature contours relates to a high temperature position. Also the blocks have higher temperature close to the base plate, which corresponds to a low convection heat transfer coefficient. It can be seen that near the top surface, temperature is close to the fin base temperature due to high thermal conductivity assumed for the fins (202 W/m k). However by decreasing the thermal conductivity of the fin, such temperature differences will be increased. It is observed that for high Reynolds number, the temperature variation over the plate surface is not significant, except at the edges, and recirculation produces a nearly uniform temperature in the wake and strong variation in the other regions. Isothermal lines have symmetric closed circles in the wake with high values in the center of the wake and gradually reduce with off-center position. Far from the blocks, the effects of the heating element on the fluid temperature reduces.

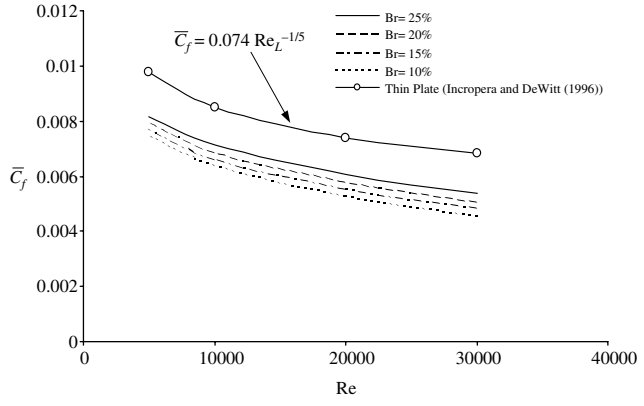

Fig. 11. Variation of average friction coefficient over the plate side surface, Hr = 5, Ar = 5.

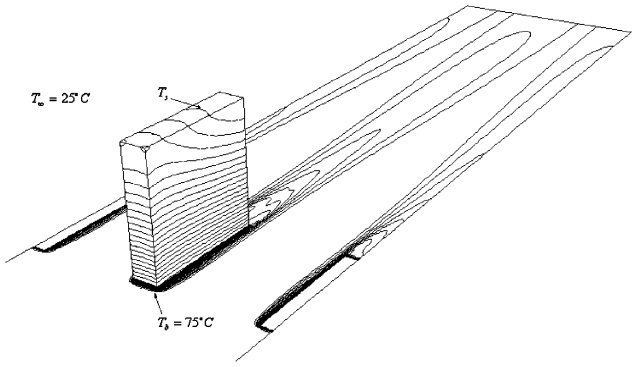

Fig. 12. Typical 3D contours of plate surface temperature, $T_b = 75$ °C, $T_\infty = 25$ °C, increment = 0.7 °C, Hr = 5, Br = 20%, $Re = 3 \times 10^4$.

Fig. 13 demonstrates 2D contours of surface Nusselt number for different Reynolds numbers. From these figures, the location of hot spots and cold spots over the fin surface can be identified. The forward and upward edges have the lowest temperature. It is also observed that the maximum Nusselt number is not exactly in the reattachment region. This value occurs in some region around the reattachment point, similar to the two-dimensional finding of Ota and Ohi (1995). Fig. 13 also demonstrates that the upper edge effect is enhanced cooling at increasing Reynolds number. Fig. 14 presents the variation of average overall Nusselt number over the entire surface of the blocks ($\overline{Nu} = \bar{h}D/\lambda$). In this figure, the experimental measurements of Sparrow et al. (1982) for an array of rectangular modules deployed along one wall of a flat rectangular duct and the results for a thin plate (Incropera and DeWitt, 1996) are also included. Consistent agreement is observed as Br is reduced by means of increasing the space between the blocks with constant thickness. From Fig. 14, it can be observed that the average Nusselt number increases with Reynolds number, or by increasing the blockage ratio (by decreasing the blocks spacing).

For practical consideration the average Nusselt number is needed. For the range of the numerical computations made in this study with a block of aspect ratio 5, a correlation for average overall Nusselt number of block is developed:

$$\overline{Nu} = 0.126Re^{0.68}(1 + 2.13\mathrm{Br}) \quad \text{for } 5 \times 10^3 \leqslant Re \leqslant 3 \times 10^4 \text{ and } 10\% \leqslant \mathrm{Br} \leqslant 25\% \quad (6)$$

The corresponding variation of correlation (6) is presented in Fig. 15, which shows good agreement with

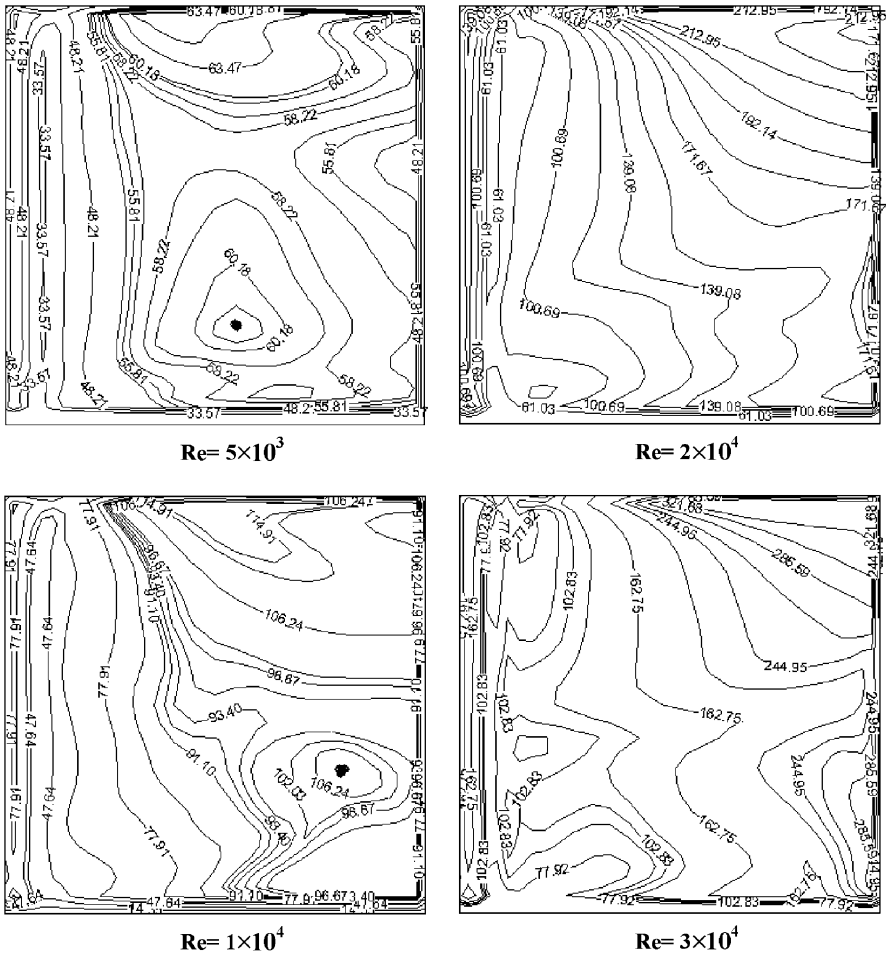

Fig. 13. Typical 2D contours of Nusselt number over the plate side surface, Hr = 5, Br = 15%, Ar = 5 ((●) region of maximum Nusselt number or cold spot).

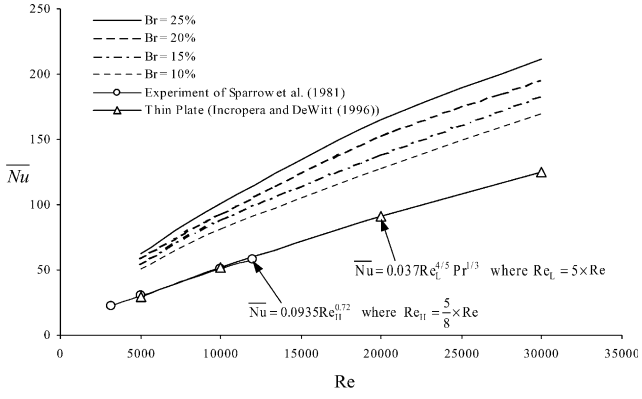

Fig. 14. Variation of average Nusselt number over the blocks, Hr = 5, Ar = 5.

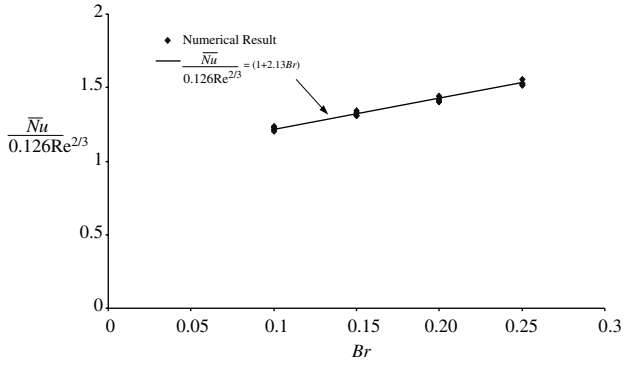

Fig. 15. Correlation of average overall Nusselt number over the block surface, Hr = 5, Ar = 5.

computed data. This expression is similar to the correlation presented for average Nusselt number by Igarashi and Mayumi (2001) in terms of variation with Reynolds number. Closing the spacing between plates enhances the local convection coefficient and the influences of upper edge and shear layer breaking or bubble breaking near the edge mixes the flow and contributes to an increase of Nusselt number.

In the present computations, the array of plates can be considered as finite fins attached over a surface such as in heat exchangers, cooling of electronic components on circuit boards, cooling of gas-turbine blades or

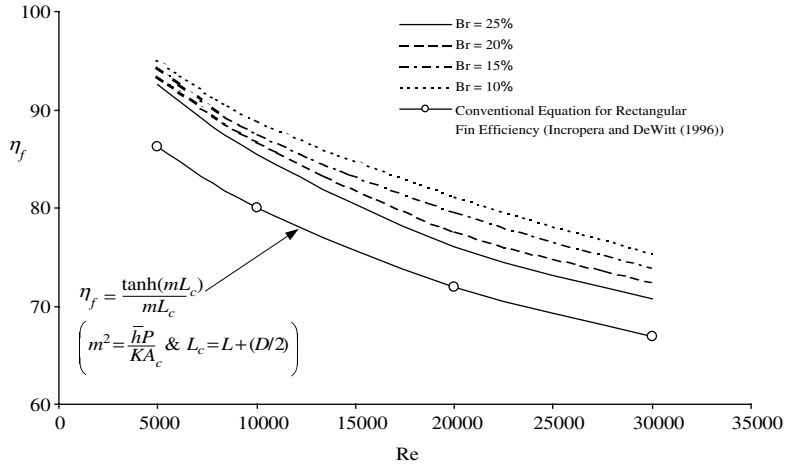

Fig. 16. Variation of the fin efficiency, Hr = 5, Ar = 5.

engines. Conjugate conduction and convection heat transfer can simulate the fins performance for various flows and fin spacings. Measurement of fin thermal performance can be provided by fin efficiency, which represents the convection heat transfer from the fin rather than the maximum driving potential for convection. The maximum rate at which a fin could dissipate energy is the rate that would exist if the entire fin surface were at the base temperature, T_b. The fin efficiency is therefore defined as:

$$\eta_{\mathrm{f}} = \frac{q_{\mathrm{f}}}{q_{\max}} = \frac{q_{\mathrm{f}}}{\bar{h}A_{\mathrm{f}}(T_{\mathrm{b}} - T_{\infty})} \tag{7}$$

From computations performed the local convection and temperature over the entire surface of the block are calculated and the rate of heat transfer q_{f}, is determined by $q_{\mathrm{f}} = \sum \bar{h}\Delta A(T_{\mathrm{s}} - T_{\infty})$. Therefore, η_{f} can be found from relation (7). The variation of the fin efficiency, η_{f} is presented in Fig. 16. This figure shows that fin efficiency is reduced by decreasing fin spacing and increasing flow Reynolds number.

Based on the numerical values obtained, a correlation for fin efficiency is determined as follows:

$$\eta_{\mathrm{f}} = 2.823Re^{-0.14}\mathrm{Br}^{-0.0526} \quad \text{for } 5\times10^3 \leqslant Re \leqslant 3\times10^4 \text{ and } 10\% \leqslant \mathrm{Br} \leqslant 25\% \tag{8}$$

This correlation fitted with a mean average of 1% deviation. Relation (8) can be used for design implementation of finite fins on engines or heat sink elements attached over a heat-source in electronic cooling. For such configurations, usually a uniform convection coefficient is suggested, while Fig. 13 indicates that there is a strong variation of convection coefficient due to swirl motion and bubble mixing with shear boundary layer. Eq. (8) also illustrates strong effects of fin spacing and predicts higher values of heat transfer from finite fins with respect to fins with long length in the streamwise direction.

6. Conclusion

Numerical computation is made to analyze fluid flow and conjugate heat transfer from finite thick plates attached over a surface. These elements can be considered to be an array of blocks or fins for various applications. Calculations are made for non-dimensional parameters Ar = 5, Hr = 5, $5\times10^3 \leqslant Re \leqslant 3\times10^4$ and $10\% \leqslant \mathrm{Br} \leqslant 25\%$ and the following conclusion are made:

1. For three-dimensional flows, separation and reattachment over the plate surfaces and recirculation downstream of the plate are highly depends on Reynolds number and plate blockage ratio.
2. The length of reattachment region enlarges with increasing Reynolds number and decreasing blockage ratio. The height of the reattachment region decreases with increasing Reynolds number and decreasing blockage ratio. Also reattachment does not occur for high Reynolds number and for low blockage ratios.
3. The average friction factor coefficient decreases with increasing Reynolds number, which is similar to the flow over flat plates. Also by increasing blockage ratio, the friction coefficient increases.
4. Local shear stress in the recirculating bubble is negative, and after the flow reattachment over the plate it is positive. Therefore the average friction coefficient ($\overline{C_{\mathrm{f}}}$) is less than the average friction coefficient over a thin plate with the same length. Moreover, effects of three-dimensionality make the flow different from two-dimensional thin plate conditions.
5. Heat transfer prediction shows a maximum value near the reattachment zone.
6. The average Nusselt number increases with increasing Reynolds number and increasing blockage ratio. The variation of overall heat transfer for an array of bluff plates with Br in the range of

$10\% \leqslant \mathrm{Br} \leqslant 25\%$ can be obtained by $\overline{Nu} = 0.126Re^{0.68}(1 + 2.13\mathrm{Br})$.

7. It is found that for any Reynolds number in the range of $5 \times 10^3 \leqslant Re \leqslant 3 \times 10^4$, by increasing the blockage ratio to 10%, the Nusselt number increases to about 21.3%. This means that the effect of the plate's spacing is very significant for the fluid flow and heat transfer around such blocks.
8. For plates acting like fins, fin efficiency is determined and the following relation is developed to predict variation of overall fin efficiency with Reynolds number and blockage ratio: $\eta_f = 2.823Re^{-0.14}\mathrm{Br}^{-0.0526}$.

Acknowledgements

Computation of the present work was carried out at the High Performance Computation Center of Shiraz University.

References

Djilali, N., Gartshore, I.S., 1991a. Turbulent flow around a bluff rectangular plate, Part 1: experimental investigation. J. Fluid Eng., ASME Trans. 113, 51–59.

Djilali, N., Gartshore, I.S., Sacludean, M., 1991b. Turbulent flow around a bluff rectangular plate, Part II: numerical predictions. J. Fluid Eng., ASME Trans. 113, 60–67.

Hwang, K.S., Sung, H.J., Hyun, J.M., 2001. An experimental study of large-scale vortices over a blunt-faced flat plate in pulsating flow. Exp. Fluid 30, 202–213.

Igarashi, T., Mayumi, Y., 2001. Fluid flow and heat transfer around a rectangular cylinder with small inclined angle (the case of a width/height ratio of a section of 5). Int. J. Heat Fluid Flow 22, 279–286.

Incropera, F.P., DeWitt, D.P., 1996. Fundamentals of Heat and Mass Transfer, fourth ed. John Wiley & Sons, Inc., New York.

Kim, K.Y., Kim, S.S., 2002. Shape optimization of rib-roughened surface to enhance turbulent heat transfer. Int. J. Heat Mass Transfer 45, 2719–2727.

Launder, B.E., Spalding, D.B., 1974. The numerical computation of turbulent flow. Comput. Methods Appl. Mech. Eng. 3, 269–289.

McCormick, D.C., Lessmann, R.C., Test, F.L., 1984. Heat transfer to separated region from a rectangular prism in a cross stream. J. Heat Transfer 106, 276–283.

Meinders, E.R., Hanjalic, K., 1999. Vortex structure and heat transfer in turbulent flow over a wall-mounted matrix of cubes. Int. J. Heat Fluid Flow 20, 255–267.

Ota, T., Kato, N., 1991. Turbulent heat transfer in a separated and reattached flow over a blunt flat plate. ASME/SSMAE Therm. Eng. Proc. 3, 191–196.

Ota, T., Ohi, N., 1995. Turbulent heat transfer in a separated and reattached flow over a blunt flat plate. ASME/JSME Therm. Eng. Conf. 1, 363–370.

Shah, R.K., Bhatti, M.S., 1987. Turbulent and transition flow convective heat transfer in ducts. In: Shah, R.K., Kakac, S., Aung, N.A. (Eds.), Handbook of Single-Phase Convection Heat Transfer. Wiley, New York.

Sparrow, E.M., Niethammer, J.E., Chaboki, A., 1982. Heat transfer and pressure drop characteristics of arrays of rectangular modules encountered in electronic equipment. Int. J. Heat Transfer 25 (7), 961–973.

Vandoormaal, J.P., Raithby, G.D., 1984. Enhancements of the simple method for predicting incompressible fluid flows. Num. Heat Transfer 7, 147–163.

Yaghoubi, M., Amnieh, H., Velayati, E., 2002. Laminar fluid flow and heat transfer from stacks of blunt fins with finite length. In: Proceedings of ESDA2002, 6th Biennial Conference on Engineering System Design and Analysis, ESDA2002/ATF-014, Istanbul, Turkey, July 8–11.

Yakhot, V., Orszag, S.A., 1986. Renormalization group analysis of turbulence. J. Sci. Comput. 1, 3–51.

Yakhot, V., Orszag, S.A., Thangam, S., Gatski, T.B., Speziale, C.G., 1992. Development of turbulence models for shear flows by a double expansion Technique. Phys. Fluids A 4 (7), 1510–1520.